Covariance Matrices for Differential and Angle-Integrated Neutron-Induced Elastic and Inelastic Scattering Cross Sections of ^{56}Fe

Shengli Chen[1,2,a], *David* Bernard[1], *Pascal* Archier[1], *Cyrille* De Saint Jean[1], *Gilles* Noguere[1], and *Pierre* Tamagno[1]

[1] CEA, Cadarache, DEN/DER/SPRC/LEPh, 13108 Saint Paul Les Durance, France
[2] Université Grenoble Alpes, I-MEP2, 38402 Saint Martin d'Hères, France

Abstract. Correlations between neutron inelastic scatterings angular distributions are not included in the Joint Evaluated Fission and Fusion (JEFF) nuclear data library, while they are key quantities for uncertainty propagation of nuclear data. By reproducing the angle-integrated cross sections and uncertainties of JEFF-3.1.1, the present work obtains covariance matrix between high energy model parameters using the least square method implemented in the CONRAD code. With this matrix, it is possible to generate correlations between angle-integrated cross sections and angular distributions, which are usually presented by Legendre coefficients. As expected, strong correlations are found, for example, between the Legendre coefficients of elastic and first-level-inelastic scatterings and the angle-integrated total, elastic, total inelastic cross sections.

1. Introduction

In the nuclear industry, both Reactor Pressure Vessels (RPVs) for Pressurized Water Reactors (PWRs) and fuel cladding in Sodium-cooled Fast Reactors (SRFs) are Stainless Steel (SS), which is also a candidate cladding material for PWR Accident Tolerant Fuel (ATF) [1], [2]. SS is mainly constituted with iron, in which the abundance of ^{56}Fe is 91.8%. Therefore, the analyses of covariance matrices of ^{56}Fe are necessary for both neutronic investigations and studies of neutron irradiation in materials.

The angular distribution of scattering reactions, called also as the differential scattering cross section, is one of the most important quantities in nuclear data evaluation. The angular distribution of neutrons determines directly the neutron spectrum. On the other hand, the recoil energy of a Primary Knock-on Atom (PKA) is deduced from the angular distributions, while the former is the basis for investigating the irradiation damage of materials.

However, the complete covariance matrices of differential scattering cross sections in the Joint Evaluated Fission and Fusion (JEFF) nuclear data libraries are not given. The present work focuses on the determination of the covariance matrix between high energy model parameters for ^{56}Fe. This matrix can be used to calculate complete covariance matrix between angle-integrated cross sections and Legendre coefficients.

[a] Corresponding author: shengli.chen@cea.fr

2. Methods

The neutron inelastic scattering threshold is 862 keV for ^{56}Fe in both JEFF-3 libraries and ENDF/B-VII libraries. The second level of inelastic scattering of ^{56}Fe starts at 2.1 MeV. Due to few experimental data for each level of inelastic scattering, the R-matrix theory [3] is no longer the best choice for neutron energy above 2 MeV. Therefore, the Optical Model (OM) and the Statistical Model (SM) are used in the present work. The Bayes' theorem is used to determine the optimized model parameters and the corresponding covariance matrix.

2.1 Optical Model

In high energy region, the OM is usually used to calculate cross sections. Morillon and Romain proposed parameters for a Dispersive Optical Model Potential (DOMP) for neutrons with incident energies from 1 keV to 200 MeV [4]:

$$U(r,E) = [V_V(E) + iW_V(E)]f(r,R,a) + [V_S(E) + iW_S(E)]g(r,R,a) + [V_{SO}(E) + iW_{SO}(E)]\frac{1}{r}\left(\frac{h}{m_\pi c}\right)^2 g(r,R,a)\mathbf{1}\cdot\boldsymbol{\sigma}, \quad (1)$$

where *V* and *W* respectively represent the real and imaginary terms of potential, the subscript *V*, *S*, *SO* respectively refer to the Volume, Surface, and Spin-Orbit parts in the DOMP. The volume shape function *f* is a Wood-Saxon form and *g* is its partial deviation to position *r*:

$$f(r,R,a) = \frac{1}{1+\exp[(r-R)/a]}. \quad (2)$$

$$g(r,R,a) = -4a\frac{d}{dr}f(r,R,a). \quad (3)$$

The same radius in Woods-Saxon form is used for different parts in the DOMP. For ^{56}Fe, the radius and the diffuseness proposed by Morillon and Romain are [4]:

$$R = 1.268A^{1/3}\ \text{(fm)}, \quad (4)$$

$$a = 0.566 + 5\times10^{-9}A^3\ \text{(fm)}, \quad (5)$$

where *A* is the nuclear mass number.

All prior parameters in the DOMP can be found in the Reference Input Parameter Library (RIPL) [5]. The OM and SM calculations are performed with the nuclear reaction code TALYS [6], in which the OM code ECIS [7] is included.

2.2 Optimization and Uncertainties of Parameters

The COde for Nuclear Reaction Analysis and Data assimilation (CONRAD) [8] is used in the present work for the data assimilation. The Bayes' theorem implicates that the posterior probability density is:

$$p\left(\vec{x}\middle|\vec{E},U\right) = \frac{p\left(\vec{E}\middle|\vec{x},U\right)p(\vec{x},U)}{\int p\left(\vec{E}\middle|\vec{x},U\right)p(\vec{x},U)d\vec{x}}, \quad (6)$$

where vector $\vec{x}$ represents the parameters in physical model, $\vec{E}$ denotes the experimental data, and *U* refers to the prior information. Under the hypothesis of Gaussian distribution for the probability density of $\vec{x}$, maximization of the posterior probability density is equivalent to minimization of the Generalized Least Square (GLS) cost function:

$$\chi^2_{GLS} = (\vec{x}-\vec{x}_0)^T M_x^{-1}(\vec{x}-\vec{x}_0) + \left(\vec{C}-\vec{E}\right)^T M_E^{-1}\left(\vec{C}-\vec{E}\right), \quad (7)$$

where $\vec{x}_0$ represents the vector containing prior values, $\vec{C}$ and $\vec{E}$ denote the calculated and experimental data, respectively. M_x (M_E resp.) stands for the covariance matrix of $\vec{x}$ ($\vec{E}$ resp.). In the present work, the cross sections in JEFF-3.1.1 [9] are used as the experimental data in

order to obtain the results corresponding to other information in JEFF-3.1.1. The Gauss-Newton scheme (known as Newton method for one-dimension solution) is used to find the minimum of the GLS cost function by iteration. The criterion of the convergence judgment is the relative variation of χ^2_{GLS}. It is set to 10^{-5} in the present work.

The parameters contained in the vector $\vec{x}$ are observable parameters. Posterior $\vec{x}$ and M_x are determined in the fitting procedure by iteration. On the other hand, nuisance parameters have also contributions to the posterior covariance matrix between observable parameters $\vec{x}$. The posterior covariance matrix between observable parameters can be expressed by [10]:

$$\Sigma_{11} = M_x + (G_x^T G_x)^{-1} G_x^T G_\theta M_\theta G_\theta^T G_x (G_x^T G_x)^{-1}. \quad (8)$$

where the matrices *G* contain partial derivation of calculated values. For $k = x, \theta$,

$$G_{k,(i,j)} = \partial C_i / \partial k_j. \quad (9)$$

More information about the data assimilation applied in the generation of covariance matrices for nuclear data can be found in Ref. [10].

An important remark is that the elastic cross sections from 850 keV up to 3.905 MeV in JEFF-3.1.1 are direct interpolations of experimental data of natural iron (Kinney's measurements [11] between 850 keV and 2.5 MeV and Smith's results [12] from 2.5 MeV to 3.905 MeV) [13]. Therefore, the OM and the SM cannot reproduce the structure in the angle-integrated cross sections of JEFF-3.1.1. The least square method implemented in CONRAD code permits to determine high energy model parameters that "mimic" the JEFF-3.1.1 evaluation.

2.3 Angular Distribution

In ENDF-6 format, the angular distribution is given by:

$$\sigma(\mu, E) = \frac{\sigma(E)}{2\pi} f(\mu, E), \quad (10)$$

where $\sigma(E)$ is the angle-integrated cross section at incident neutron energy *E*, and the normalized probability distribution is expressed by:

$$f(\mu, E) = \sum_{l=0}^{NL} \frac{2l+1}{2} a_l(E) P_l(\mu), \quad (11)$$

where μ is the cosine of neutron emission angle, P_l is the *l*-th order Legendre polynomial, a_l is the coefficient of Legendre polynomial stored in the ENDF, *NL* (≤64) is the highest order of Legendre polynomial. *NL* increases with incident energy due to more forward-oriented angular distribution for higher energy (e.g. 4 at low incident energy and up to 20 at high energy in JEFF-3.1.1). Because the integral of P_l ($l > 0$) over [-1,1] is null and that of P_0 is 2, one can conclude that $a_0(E) = 1$. It is not necessary to store a_0 or to analyze its uncertainty.

3. Results and Discussion

3.1 Reproduction of cross sections

Figure 1 shows the ^{56}Fe total and first-level-inelastic scattering cross sections of JEFF-3.1.1 (dashed line) and the results with corresponding uncertainties calculated by the OM and the SM with optimized parameters. The fluctuations from experimental data of JEFF-3.1.1 cannot be reproduced by the OM and the SM, but the global correspondence between our results and JEFF-3.1.1 is ensured, especially for incident energy above 6 MeV. It is noticeable that the OM parameters should be improved to compute the cross sections below 4 MeV for ^{56}Fe. However, such an approach is sufficient for producing suitable covariance information for nuclear applications on atomic displacement and fast neutron flux in RPVs.

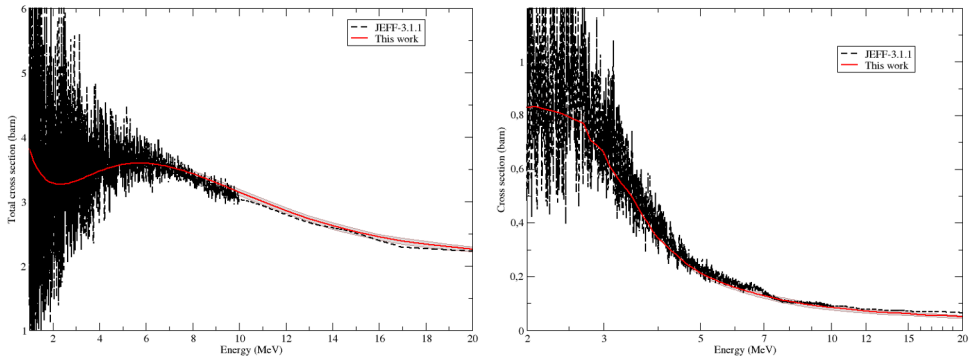

Figure 1. Total (left) and first-level-inelastic scattering (right) cross sections of JEFF-3.1.1 (dashed line) and the cross sections with corresponding uncertainties obtained in the present work

3.2 Correlation matrices

The correlation matrices presented in the present work are from neutron energy of 860 keV up to 20 MeV with logarithm scale. Figure 2 shows the correlation matrices between angle-integrated cross sections, including the total cross section (MT1), elastic scattering cross section (MT2), total inelastic scattering cross sections (MT4), first- to third-level-inelastic scattering cross sections (MT51 to MT53), and the continuum inelastic scattering (MT91). Figure 3 (Figure 4 resp.) illustrates the correlations between angle-integrated cross sections and the Legendre coefficients of elastic (first-level-inelastic resp.) scattering. Figure 5 presents the correlations between Legendre coefficients from the 1st order to the 5th order for MT51. Figure 6 reveals the correlations of Legendre coefficients between MT2 and MT51.

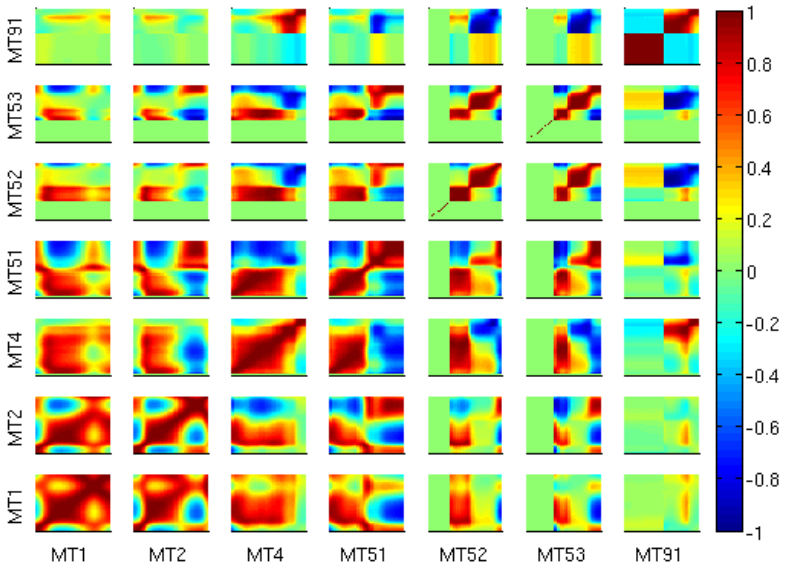

Figure 2. Correlation matrices between different angle-integrated cross sections denoted by the corresponding MT numbers

In Figure 2, the existence of correlations with MT91 at low energy is due to the low incident threshold energy of the MT91 reaction in TALYS. It has no influence on the application because of the negligible MT91cross sections between the threshold in TALYS

and that in evaluated libraries. The results are in agreement with the expectation because: (a) MT1 is the sum of all cross sections and MT2 is predominant at low energy; (b) MT4 is the sum of MT51 to MT80 plus MT91, while MT51 has the most important contribution at low energy and MT91 dominates at high energy.

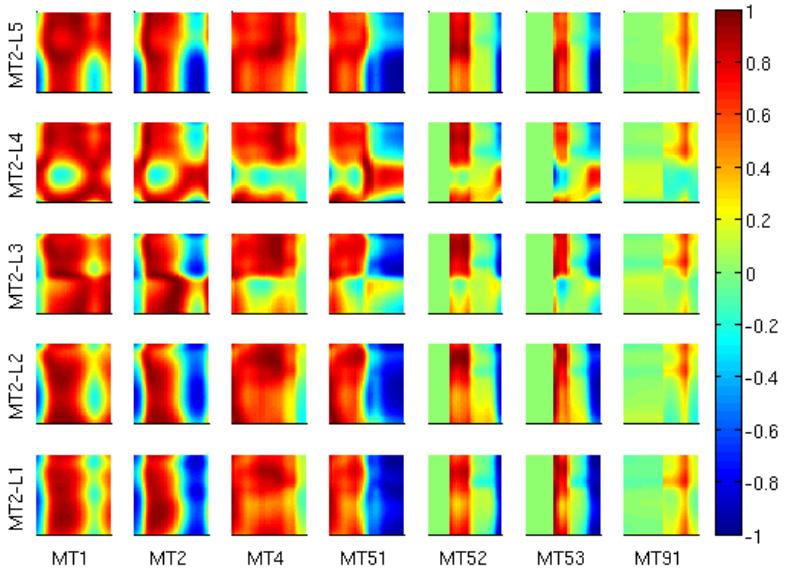

Figure 3. Correlation matrices between cross sections and Legendre coefficients of elastic scattering

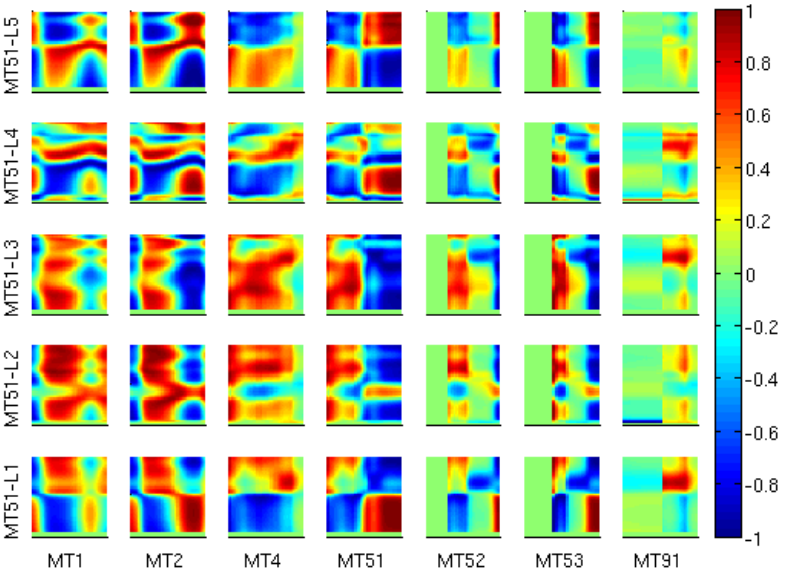

Figure 4. Correlation matrices between angle-integrated cross sections and Legendre coefficients of first-level-inelastic scattering

Strong correlations are found between angle-integrated cross sections and low-order Legendre coefficients for MT2 (Figure 3). The correlations of Legendre coefficients of MT2 and angle-integrated cross sections of MT4 are important within the OM and the SM. However, weak correlations exist between MT2 and MT91 for both differential and angle-integrated cross sections (Figure 2 and Figure 3). Comparing with MT2 (Figure 3), the

Legendre coefficients of MT51 have less strong correlations with angle-integrated cross sections (shown in Figure 4).

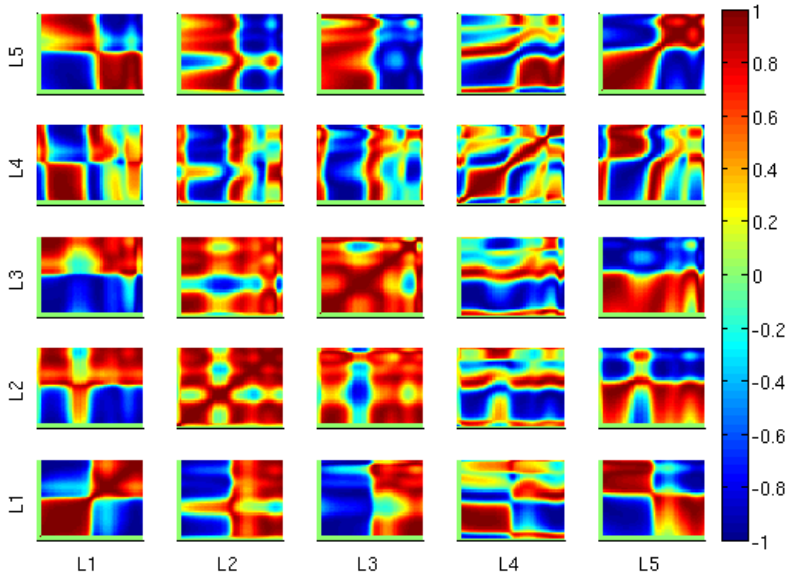

Figure 5. Correlation matrices between Legendre coefficients from the 1st to the 5th order for the first-level-inelastic scattering

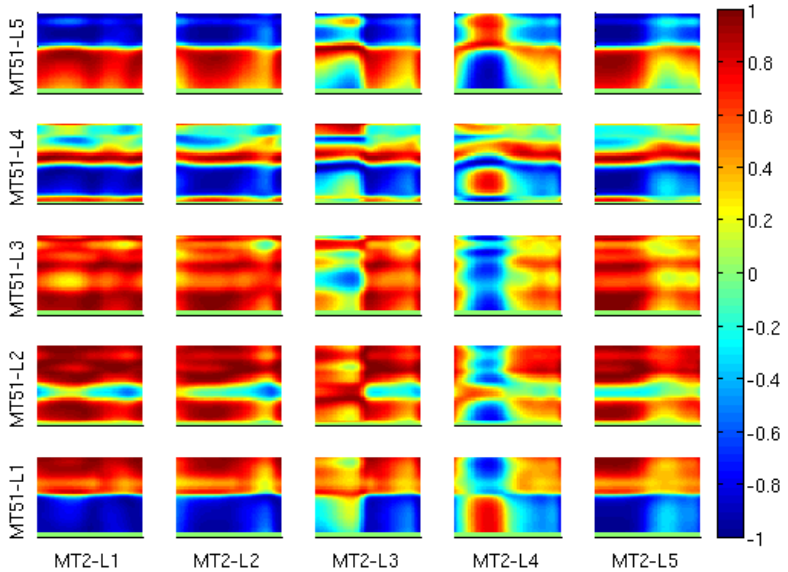

Figure 6. Correlation matrices of Legendre coefficients between the elastic scattering and the first-level-inelastic scattering

From Figure 5, one can conclude that the correlations between Legendre coefficients are of great importance for the first-level-inelastic scattering. It is noticeable that the correlations between Legendre coefficients for elastic scattering is even stronger. Figure 6 shows the strong correlations between low-order Legendre coefficients of MT2 and those of MT51. Therefore, correlations between differential and angle-integrated cross sections should be

considered in nuclear applications, such as the uncertainty quantification for fast neutron fluence investigated in Ref. [14].

4. Conclusions

Thanks to the least square method implemented in the CONRAD code, we succeed to reproduce the n+^{56}Fe angle-integrated cross sections and uncertainties of JEFF-3.1.1 with the optical model (ECIS) and the statistical model (TALYS). Correlations between all angle-integrated cross sections and differential scattering cross sections are obtained. Strong correlations are found between angle-integrated cross sections and differential cross sections. The obtained covariance matrices between differential and angle-integrated cross sections are useful for further applications on uncertainty quantification of neutron fluence in reactor pressure vessels and neutron-induced irradiation damage of materials containing ^{56}Fe.

5. References

[1] S. Chen and C. Yuan, "Neutronic Analysis on Potential Accident Tolerant Fuel-Cladding Combination U_3Si_2-FeCrAl," *Sci. Technol. Nucl. Install.*, vol. 2017, p. 3146985, 2017.

[2] S. Chen, C. Yuan, and D. Guo, "Radial distributions of power and isotopic concentrations in candidate accident tolerant fuel U_3Si_2 and UO_2/U_3Si_2 fuel pins with FeCrAl cladding," *Ann. Nucl. Energy*, vol. 124, pp. 460–471, Feb. 2019.

[3] A. M. Lane and R. G. Thomas, "R-Matrix Theory of Nuclear Reactions," *Rev. Mod. Phys.*, vol. 30, no. 2, pp. 257–353, Apr. 1958.

[4] B. Morillon and P. Romain, "Dispersive and global spherical optical model with a local energy approximation for the scattering of neutrons by nuclei from 1 keV to 200 MeV," *Phys. Rev. C*, vol. 70, no. 1, p. 014601, Jul. 2004.

[5] R. Capote *et al.*, "RIPL – Reference Input Parameter Library for Calculation of Nuclear Reactions and Nuclear Data Evaluations," *Nucl. Data Sheets*, vol. 110, no. 12, pp. 3107–3214, Dec. 2009.

[6] A. J. Koning, S. Hilaire, and M. C. Duijvestijn, "TALYS-1.8," in *International Conference on Nuclear Data for Science and Technology*, 2007, pp. 211–214.

[7] J. Raynal, "ECIS code, distributed by the NEA DATA Bank," Paris, France, 2003.

[8] P. Archier *et al.*, "CONRAD Evaluation Code: Development Status and Perspectives," *Nucl. Data Sheets*, vol. 118, no. Supplement C, pp. 488–490, 2014.

[9] A. Santamarina *et al.*, "The JEFF-3.1.1 Nuclear Data Library," OECD/NEA, JEFF Report 22, NEA No. 6807, 2009.

[10] G. Noguere, P. Archier, C. D. S. Jean, and B. Habert, "Zero Variance Penalty Model for the Generation of Covariance Matrices in Integral Data Assimilation Problems," *Nucl. Sci. Eng.*, vol. 172, no. 2, pp. 164–179, 2012.

[11] W. E. Kinney and J. W. McConnell, "High Resolution Neutron Scattering Experiments at ORELA," in *Int.Conf.on Interact.of Neutr.with Nuclei*, Lowell, USA, 1976, p. 1319.

[12] A. Smith and P. Guenther, "Scattering of MeV Neutrons from Elemental Iron," *Nucl. Sci. Eng.*, vol. 73, p. 186, 1980.

[13] C. Vaglio-Gaudard, "Validation of iron nuclear data for the neutron calculation of nuclear reactors," PhD Thesis, Grenoble INP, 2010.

[14] L. Clouvel, P. Mosca, and J. M. Martinez, "Uncertainty propagation of double-differential scattering cross section in fast fluence calculation for the PWR surveillance capsules," presented at the PHYSOR 2018, Cancun, Mexico, 2018.